

Measurement of the front-end dead-time of the LHCb muon detector and evaluation of its contribution to the muon detection inefficiency

L. Anderlini^a, M. Anelli^b, F. Archilli^c, G. Auriemma^{d,e}, W. Baldini^{c,f}, G. Bencivenni^b, A. Bizzeti^{a,g}, V. Bocci^d, N. Bondar^{c,h}, W. Boniventoⁱ, B. Bochun^h, C. Bozzi^{c,f}, D. Brunduⁱ, S. Cadedduⁱ, P. Campana^b, G. Carboni^{j,k}, A. Cardiniⁱ, M. Carletti^b, L. Casuⁱ, A. Chubykin^h, P. Ciambone^b, E. Dané^b, P. De Simone^b, A. Falabella^l, G. Felici^b, M. Fiore^{c,f,m}, M. Fontanaⁱ, P. Fresch^d, E. Furfaro^{j,k}, G. Graziani^a, A. Kashchuk^h, S. Kotriakhova^h, A. Laiⁱ, G. Lanfranchi^b, A. Loiⁱ, O. Maev^h, G. Mancaⁿ, G. Martellotti^d, P. Neustroev^h, R.G.C. Oldeman^{i,o}, M. Palutan^b, G. Passaleva^a, G. Penso^{d,p}, D. Pinci^{d,*}, E. Polycarpo^q, B. Saitta^{i,o}, R. Santacesaria^d, M. Santimaria^b, E. Santovetti^{j,k}, A. Saputi^b, A. Sarti^{b,p}, C. Satriano^{d,e}, A. Satta^j, B. Schmidt^c, T. Schneider^c, B. Sciascia^b, A. Sciubba^{d,p}, B.G. Siddi^f, G. Tellarini^{f,m}, C. Vacca^{c,i}, R. Vazquez-Gomez^b, S. Vecchi^f, M. Veltri^{a,r} and A. Vorobyev^h

^aSezione INFN di Firenze, Firenze, Italy

^bLaboratori Nazionali dell'INFN di Frascati, Frascati, Italy

^cEuropean Organization for Nuclear Research (CERN), Geneva, Switzerland

^dSezione INFN di Roma La Sapienza, Roma, Italy

^eUniversità della Basilicata, Potenza, Italy

^fSezione INFN di Ferrara, Ferrara, Italy

^gUniversità di Modena e Reggio Emilia, Modena, Italy

^hPetersburg Nuclear Physics Institute (PNPI), Gatchina, Russia

ⁱSezione INFN di Cagliari, Cagliari, Italy

^jSezione INFN di Roma Tor Vergata, Roma, Italy

^kUniversità di Roma Tor Vergata, Roma, Italy

^lCNAF-INFN, Bologna, Italy

^mUniversità di Ferrara, Ferrara, Italy

ⁿLAL, Université Paris-Sud, CNRS/IN2P3, Orsay, France

^oUniversità di Cagliari, Cagliari, Italy

^pUniversità di Roma La Sapienza, Roma, Italy

^qUniversidade Federal do Rio de Janeiro (UFRJ), Rio de Janeiro, Brazil

^rUniversità di Urbino, Urbino, Italy

* Corresponding author.

E-mail: davide.pinci@roma1.infn.it

ABSTRACT: A method is described which allows to deduce the dead-time of the front-end electronics of the LHCb muon detector from a series of measurements performed at different luminosities at a bunch-crossing rate of 20 MHz. The measured values of the dead-time range from ~ 70 ns to ~ 100 ns. These results allow to estimate the performance of the muon detector at the future bunch-crossing rate of 40 MHz and at higher luminosity.

KEYWORDS: Front-end electronics for detector readout; Dead-time; Wire chambers; Muon spectrometers.

Contents

1. Introduction	1
2. Measurement of the CARIOCA dead time with background events	2
2.1 Dead-time with random particles	2
2.2 Dead-time with bunched particles	3
2.3 Monte Carlo simulation of background events	4
2.3.1 Probability distribution function of the number of hitting particles	4
2.3.2 Time distribution of the background hits	5
2.4 Background Monte Carlo results	5
2.5 Experimental results	6
3. Front-end inefficiency for muon detection due to CARIOCA dead-time	9
3.1 Muon Monte Carlo simulation	10
3.2 Muon Monte Carlo results	10
3.3 Muon hit inefficiency in the past and future running conditions	11
4. Conclusions	13
A. Dead-time effect on background counting and muon detection	14

1. Introduction

The muon detector of the LHCb experiment [1–3] is composed of 5 stations (M1–M5) placed along the beam axis. Each station is divided in 4 regions (R1–R4), with increasing distance from the beam pipe. Multiwire proportional chambers (MWPC) are used everywhere, except in the most irradiated region R1 of station M1 where triple-GEM [4, 5] were adopted. The detector comprises 1380 chambers with 122112 readout channels. Each chamber is segmented in anode and/or cathode elements named *pads*. In the front-end (FE), each pad is read-out by a CARIOCA chip [6] which performs the signal amplification, shaping and discrimination. In the first data taking period (years 2009-2013) the LHCb experiment ran at a luminosity of up to $4 \times 10^{32} \text{ cm}^{-2}\text{s}^{-1}$ and at a bunch-crossing (BC) rate $R_0 = 20 \text{ MHz}$. To investigate the performance of the muon detector at the future BC rate of 40 MHz and at higher luminosity, the knowledge of the dead-time of the CARIOCA is crucial.

The present paper is divided in two parts. In the first part (Section 2) we describe the method adopted to deduce the dead-time of the CARIOCA (δ_c) from a measure of background rates (R^*) at different luminosities. These measurements were performed in dedicated runs with a non-standard data acquisition (DAQ).

In the second part of this paper (Section 3) the values of δ_c obtained in Section 2 are used to evaluate the muon detection inefficiency due to the CARIOCA dead-time when the experiment runs in the standard data taking conditions and at a BC rate of 20 MHz and 40 MHz.

2. Measurement of the CARIOCA dead time with background events

To determine the CARIOCA dead-time, the behaviour of the FE electronics was measured in dedicated runs at $\sqrt{s} = 8$ TeV, at a BC rate of 20 MHz and at five different luminosities: $L_1 = 4 \times 10^{32}$, $L_2 = 5 \times 10^{32}$, $L_3 = 6 \times 10^{32}$, $L_4 = 8 \times 10^{32}$ and $L_5 = 1 \times 10^{33} \text{ cm}^{-2}\text{s}^{-1}$. In these runs, background events were counted by free-running scalers placed in each FE board, downstream of the discriminator. These scalers are asynchronous with the LHC clock and can be controlled remotely. The dead-time of the scalers is negligible compared with that of the CARIOCA.

The measurements were performed on the readout channels of the most irradiated MWPCs belonging to stations M1 and M2. The counting rates of these channels are mainly due to low energy background particles. The contribution of the electronic noise to the measured rate was evaluated without beams and found to be negligible.

2.1 Dead-time with random particles

If the time distribution of the particles hitting a pad would not have any particular time structure, the counting rate (R^*) of a given readout channel would be given by:

$$R^* = R_{part}(1 - \delta_c R^*) \quad (2.1)$$

where δ_c is the CARIOCA dead time and R_{part} is the rate of hitting particles.

If R^* is measured at a single luminosity, the value of δ_c cannot be deduced from Eq. 2.1 because R_{part} is unknown. Two measurements (R_i^* and R_j^*) performed at two different luminosities (L_i and L_j) are necessary. For each of them Eq. 2.1 becomes:

$$\begin{cases} R_i^* = R_{part}^{(i)}(1 - \delta_c R_i^*) \\ R_j^* = R_{part}^{(j)}(1 - \delta_c R_j^*) \end{cases} \quad (2.2)$$

For each pad the ratio ρ_{ij} , which can be evaluated from the experimental data, is defined [7]:

$$\rho_{ij} = \frac{R_j^*/L_j}{R_i^*/L_i} \quad (L_i < L_j) \quad (2.3)$$

Taking into account that R_{part} is proportional to the luminosity ($R_{part}^{(i)}/R_{part}^{(j)} = L_i/L_j$), Eqs. 2.2 and 2.3 result in the following expression:

$$\rho_{ij} = 1 - \delta_c(1 - \beta_{ij})R_j^* \quad (\beta_{ij} = L_i/L_j < 1) \quad (2.4)$$

For each pad of the detector, ρ_{ij} and R_j^* can be measured and reported on a bi-dimensional scatter plot. According to Eq. 2.4, the points of this plot should be aligned with a slope equal to $\delta_c(1 - \beta_{ij})$. Therefore the measured value of this slope allows to evaluate δ_c .

For particles arriving at random times, the number of hits on a pad (N_0) in a time interval Δt follows a Poisson distribution:

$$P_0(N_0) = \frac{1}{N_0!} e^{-R_{part}\Delta t} (R_{part}\Delta t)^{N_0} \quad (2.5)$$

and the interarrival times (τ) obey an exponential distribution:

$$P(\tau) = R_{part} e^{-R_{part} \tau} \quad (2.6)$$

With bunched particles this interarrival distribution is modified and the distribution of the number of hitting particles in a given time interval is no longer given by Eq. 2.5.

In the next section the real experimental situation will be considered.

2.2 Dead-time with bunched particles

In the measurements performed at the LHC collider, R_{part} has a bunched time structure which reflects the sequence of the bunch crossings. Long trains of consecutive BCs occurring every 25 ns ($R_0 = 40$ MHz) or 50 ns ($R_0 = 20$ MHz) are followed by empty intervals with no BCs. The overall duty cycle is $\sim 70\%$. Moreover there is a finite probability that more than one particle generated in the same interaction will hit, near in time, the same pad, dependently on its size and position and independently of luminosity.

A relation similar to Eq. 2.1 can still be written but δ_c must be replaced by an ‘‘effective dead-time’’ δ_{eff} :

$$R^* = R_{part}(1 - \delta_{eff}R^*) \quad (2.7)$$

where R^* and R_{part} are the rates during the BC trains.

The value of δ_{eff} depends on:

- the CARIOCA dead-time δ_c ,
- the repetition rate of the BCs (20 MHz or 40 MHz),
- the probability distribution function (pdf) of the number of particles (N_{part}) arriving on the pads for each BC (the pdf changes with the luminosity),
- the time of arrival of particles on the pad,
- the time fluctuations of the chamber and FE response.

The method described in Sec. 2.1 can still be applied provided the dependence of δ_{eff} on the luminosity is taken into account. Eqs.2.2 becomes:

$$\begin{cases} R_i^* = R_{part}^{(i)}(1 - \delta_{eff}^{(i)}R_i^*) \\ R_j^* = R_{part}^{(j)}(1 - \delta_{eff}^{(j)}R_j^*) \end{cases} \quad (2.8)$$

By introducing these equations in ρ_{ij} defined by Eq. 2.3, Eq. 2.4 is replaced by the relation:

$$\rho_{ij} = 1 - (\delta_{eff}^{(j)} - \delta_{eff}^{(i)}\beta_{ij})R_j^* \quad (2.9)$$

As described in the previous section, ρ_{ij} and R_j^* are measured for each pad and their values are reported on a bi-dimensional scatter plot. According to Eq. 2.9 the slope of a linear fit to this plot is equal to $\delta_{eff}^{(j)} - \delta_{eff}^{(i)}\beta_{ij}$, an expression which therefore is computable from experimental data. To evaluate δ_c from this slope, the dependence of δ_{eff} on the luminosity and on δ_c has been estimated by a Monte Carlo (MC) simulation.

2.3 Monte Carlo simulation of background events

The MC simulates the time of arrival of the pulses during a large number of consecutive BCs. If two events have a time distance lower than the CARIOCA dead-time δ_c ¹, the second one is lost. For each BC the pdf of the number of particles hitting a pad (N_{part}) and their experimental time distribution are considered.

2.3.1 Probability distribution function of the number of hitting particles

The number of background particles N_{part} hitting a pad in a BC depends on the number of p-p interactions (n_{int}) in the BC and on the number of particles (n_{part}) hitting the pad for a single p-p interaction.

At a given luminosity, n_{int} follows a Poisson statistics with a mean value² μ :

$$P_1(n_{int}) = \frac{e^{-\mu} \mu^{n_{int}}}{n_{int}!} \quad (2.10)$$

For a single p-p interaction, the number of particles (n_{part}) crossing a pad follows also a Poisson distribution with a mean value ω :

$$P_2(n_{part}) = \frac{e^{-\omega} \omega^{n_{part}}}{n_{part}!} \quad (2.11)$$

The value of ω represents the pad occupancy per interaction. It is characteristic of each pad and depends on its size and on its position in the detector. The ω values are spread over several orders of magnitude and a maximum value of ~ 0.05 was measured on M2R1.

For a single BC generating an arbitrary number of interactions, the distribution $P_3(N_{part})$ of the number of particles crossing a given pad follows a ‘‘bi-Poisson’’ distribution which results from the convolution of $P_1(n_{int})$ and $P_2(n_{part})$:

$$P_3(N_{part}) = \begin{cases} \sum_{n_{int}=1}^{\infty} \left(\frac{e^{-\mu} \mu^{n_{int}}}{n_{int}!} \right) \left(\frac{e^{-n_{int}\omega} (n_{int}\omega)^{N_{part}}}{N_{part}!} \right) & (N_{part} > 0) \\ \sum_{n_{int}=1}^{\infty} \left(\frac{e^{-\mu} \mu^{n_{int}}}{n_{int}!} \right) \left(\frac{e^{-n_{int}\omega} (n_{int}\omega)^{N_{part}}}{N_{part}!} \right) + e^{-\mu} & (N_{part} = 0) \end{cases} \quad (2.12)$$

Because the two variables n_{int} and n_{part} are uncorrelated, the average value (\bar{N}_{part}) of $P_3(N_{part})$ is equal to the product of the average values of $P_1(n_{int})$ and $P_2(n_{part})$:

$$\bar{N}_{part} = \omega \mu \quad (2.13)$$

and the background particle rate is:

$$R_{part} = R_0 \bar{N}_{part} = R_0 \mu \omega \quad (2.14)$$

¹ A gaussian fluctuation of ± 9 ns (rms) around δ_c was assumed for each event. Therefore δ_c represents the average CARIOCA dead-time. This fluctuation was estimated by laboratory tests.

²The luminosity L is proportional to μ . At $L = 4 \times 10^{32} \text{ cm}^{-2}\text{s}^{-1}$ and at a BC rate of 20 MHz, the value $\mu = 1.7$ was assumed.

In the MC, N_{part} was extracted for each BC according to the distribution given by Eq. 2.12. Note that this distribution, accounting for the probability that more particles generated in the same interaction will hit the same pad, implies that, in presence of a dead time, the inefficiency $(R_{part} - R^*)/R_{part} = \delta_{eff}R^*$ (see Eq. 2.7) will not go to zero for $\mu \rightarrow 0$, while R^* will go to zero. Therefore δ_{eff} , as defined in Eq. 2.7, will tend to infinity for $\mu \rightarrow 0$. This issue will be resumed later and discussed in Appendix A.

2.3.2 Time distribution of the background hits

The time distribution of the signals depends essentially on the time of flight of the detected particles and on the fluctuations of the response of the chamber and its readout electronics. This distribution was extracted from measurements performed in special low luminosity runs where events were acquired in a time gate of 125 ns around the triggered BC (instead of 25 ns adopted in the standard data taking) [2, 3]. Different time distributions were measured in different detector zones.

In the MC, for each BC, the hits were distributed in time according to the spectrum of Fig. 1 (full line). The band around this line includes the experimental time distributions measured in different chambers. The upper and lower bounds of this band were obtained by stretching ($\pm 10\%$) and shifting (± 2.5 ns) the full line of Fig. 1. The width of the band will be relevant to calculate the systematic errors on δ_c .

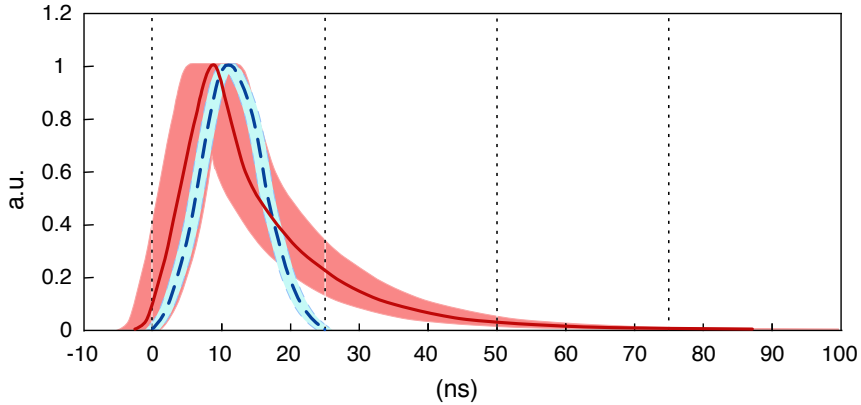


Figure 1. Full line: time distribution of the background hits in a single BC used in the MC. The band around the line represents the variation of the distributions in the different chambers (see text). Dashed line: time distribution of the muon hits. The width of the band around the dashed line corresponds to a shift of ± 1 ns. The interval between two consecutive BCs can be 50 ns ($R_0 = 20$ MHz) or 25 ns ($R_0 = 40$ MHz).

2.4 Background Monte Carlo results

Once μ , ω and δ_c are fixed, the MC determines the fraction of background hits which survive the dead-time. The value of δ_{eff} is then deduced from Eq. 2.7. The dependence of δ_{eff} on μ and δ_c , as calculated by the MC, is shown in Figs. 2a and 2b for different values of ω , δ_c and μ . The results reported in Fig. 2 show that the effective dead-time increases at low luminosity (i.e. at low μ) while at high luminosity it tends to δ_c ³. The value of δ_{eff} does not depend on ω , being the same

³As anticipated in Section 2.3.1, this behaviour is connected with the bi-poissonian pdf of R_{part} . A further discussion on the matter is reported in Appendix A.

for all pads. The undulation of the curves of Fig. 2b reflects the bunched structure of the beams. The dependence of δ_{eff} on δ_c and on μ (Fig. 2b) allows to calculate the expression $\delta_{eff}^{(j)} - \delta_{eff}^{(i)}\beta_{ij}$ and to find the value of δ_c for which this expression assumes its experimental value (Eq. 2.9).

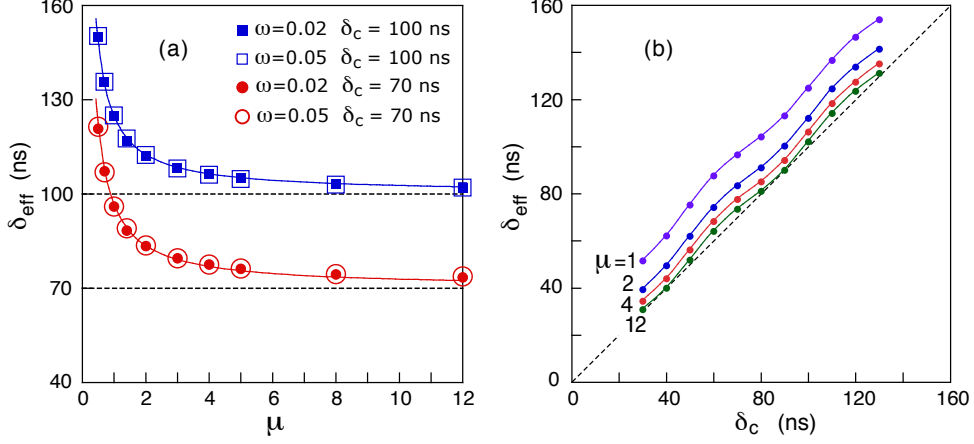


Figure 2. MC results: (a) Values of δ_{eff} as a function of μ for two values of ω and δ_c . (b) Values of δ_{eff} as a function of δ_c for four values of μ .

2.5 Experimental results

The counting rates of the pads belonging to the regions of station M1 and M2 equipped with MWPCs were measured in 1 s by the scalers of the CARIOCA chip. To take into account the duty cycle of LHC, the values of R^* were obtained by attributing the scaler counts to a time interval of 0.7 s. The measurements were performed at five different luminosities. Only the couples of measurements performed in the same day were chosen for the analysis⁴. The data belonging to the five selected pairs of luminosities (L_i, L_j) were represented on a scatter plot ρ_{ij} versus R_j^* .

As an example we show (Fig. 3a) the results of the measurements performed on all the pads of station M2, and using the pair of luminosities (L_1, L_3). Each point corresponds to a pad. Cathode and anode pads are shown separately. The difference in the slope for cathode and anode readout is mainly due to the CARIOCA chip which is slightly different for positive and negative pulses. The width of the bands is compatible with the expected statistical fluctuations on the number of counted pulses. The fluctuations are larger in regions R3 and R4 (Fig. 3a) where the counting rate is lower. The points averaged in bins of R_3^* , are reported in Fig. 3b. If no dead time effect was present, the points of Fig. 3a and 3b should be aligned around the line $\rho_{13} = 1$. The experimental points are instead distributed around a line with a non-zero slope which, according to Eq. 2.9, is equal to $\delta_{eff}^{(3)} - \delta_{eff}^{(1)}\beta_{13}$.

The procedure described for the pair of luminosities (L_1, L_3) was applied to all the pairs of luminosities considered, separately for different regions and readout. Then the MC results shown

⁴Larger variations are observed on data taken at the same nominal luminosity in different days. This effect is probably due to the uncertainty on the true luminosity value.

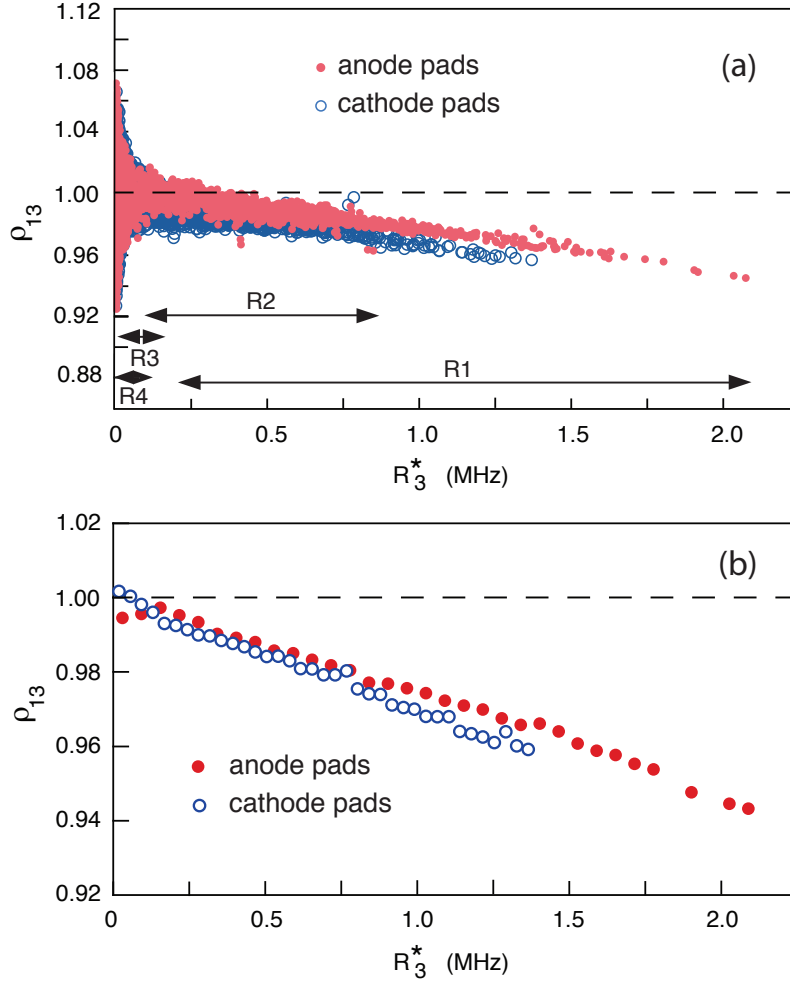


Figure 3. (a): Experimental values of ρ_{13} as a function of R_3^* (see Eq. 2.9). Each point corresponds to a pad of station M2. Anode and cathode pads are shown separately. The ranges of rate measured in the regions R1–R4 are indicated. (b): The points reported in (a) were averaged in bins of R_3^* .

in Fig. 4 allow to calculate δ_c from the measured values of $\delta_{eff}^{(j)} - \delta_{eff}^{(i)} \beta_{ij}$. The results are reported in Table 1, for the MWPCs of station M1 (regions R2, R3 and R4) and M2 (regions R1 and R2), and for cathode and anode readout separately.

For each region and readout, the δ_c values obtained from different pairs of luminosity are significantly different. The dispersion of these values, reported as the first error in the last column of Table 1, represents the main contribution to the systematic error on δ_c .

The second error is due to the uncertainties on the time distributions. To evaluate this contribution, the time distribution of the background pulses was moved inside the band shown in Fig. 1 and the maximum variation was taken. Also the fluctuation of the CARIOCA dead-time around its average value δ_c was varied in the interval 9 ± 4 ns (see footnote 1). This last variation has a small effect on the results.

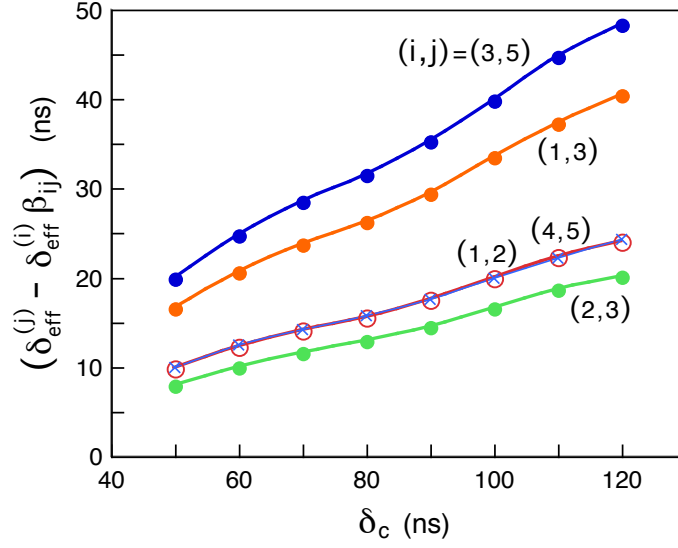


Figure 4. Slope of the linear dependence of ρ_{ij} vs. R_j^* described by Eq. 2.9. The curves, calculated with the MC, refer to the five pairs of luminosities (L_i, L_j) considered in the data analysis.

Table 1. Experimental results on the dead-time δ_c (ns) of the FE electronics of the MWPCs belonging to stations M1 and M2. The results, reported in columns 3 – 7, refer to the pair of luminosities (L_i, L_j) used. The average value of the data obtained with the five pairs of luminosities is reported in the last column. The first error is the dispersion (rms) of these values. The second error reflects the uncertainty on the time distributions (see text). The capacitance of the pads belonging to each region and readout is reported in column 2.

Region & readout	C_{pad} (pF)	(L_1, L_2)	(L_2, L_3)	(L_1, L_3)	(L_3, L_5)	(L_4, L_5)	average
M1 R2 cathode	58	101	102	97	104	106	$102 \pm 4 \pm 1$
M1 R3 cathode	51	89	90	90	93	94	$91 \pm 2 \pm 2$
M1 R4 anode	107	66	66	70	75	76	$71 \pm 4 \pm 1$
M2 R1 cathode	131	86	88	95	83	84	$87 \pm 4 \pm 2$
M2 R1 anode	75	76	77	84	62	66	$73 \pm 7 \pm 1$
M2 R2 cathode	111	82	84	84	76	83	$82 \pm 3 \pm 2$
M2 R2 anode	77	–	–	–	71	65	$68 \pm 3 \pm 2$

The results referring to the same pad type (anode or cathode) of a given station and region, but obtained with different pairs of luminosities are in a reasonably good agreement. The dead-time of the cathode readout are systematically larger than those of the anode readout. Considering separately the anode and cathode readout, some spread is still present between the results belonging to different stations and regions. This can be due to different detector geometries and therefore capacitances.

Once δ_c is determined, the values of δ_{eff} can be evaluated (Fig.2b). Finally, Eqs. 2.7 and 2.14 allow to calculate, for each pad, the corresponding value of ω . As an example the dependence of

the pad occupancy per interaction ω on R^* is shown in Fig. 5 separately for anode and cathode pads of station M2, for two luminosities L_1 and L_3 .

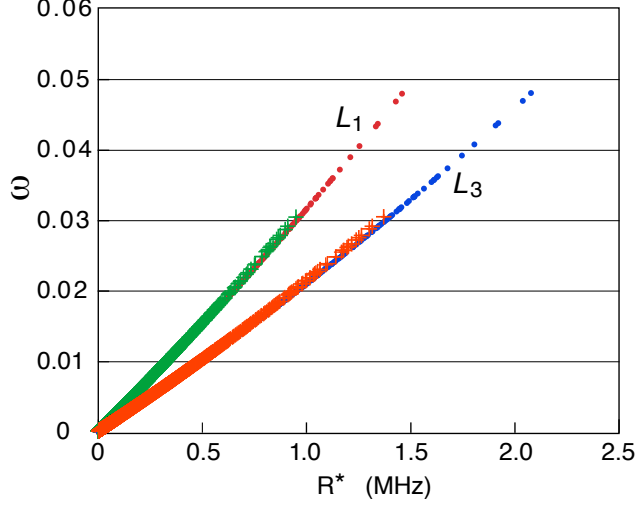


Figure 5. Experimental average number of background particles hitting a pad for one p-p interaction (ω) as a function of the pad counting rate for the two luminosities L_1 and L_3 . Each point represents a pad of station M2: full points for anode pads, crosses for cathode pads.

3. Front-end inefficiency for muon detection due to CARIOCA dead-time

Once δ_c is determined with the described method, the detection inefficiency for muon hits of each front-end⁵ due to the CARIOCA dead-time can be evaluated. In the standard data taking the hits are acquired in a 25 ns gate, corresponding to the triggered BC. If one or more particles (muon or background particles) hit the pad in the 25 ns gate, and at least one survives to the dead-time generated in a preceding BC the pad is efficient.

For a given pad the muon rate is negligible compared to the background rate so that the muon detection inefficiency is due to the dead-time generated by background hits. This inefficiency can be represented by an effective dead-time for muons ($\delta_{eff}^{(muon)}$) defined by the equation:

$$\frac{R_{muon}^*}{R_{muon}} = 1 - \delta_{eff}^{(muon)} R^* \quad (3.1)$$

⁵The MWPCs comprise two layers (1 gas gap per layer in M1 and 2 gas gaps per layer in M2). Each layer is readout by one FE (one CARIOCA chip) and the two layers are OR-ed. The inefficiency we are speaking about is the one of a hit in a single layer. To evaluate the overall muon detection inefficiency of a station, the cluster size and the correlation of the hits in the two layers must be taken into account.

where R_{muon} is the true muon rate while R_{muon}^* is the measured muon rate. The first member of Eq. 3.1 represents the FE muon detection efficiency (ϵ_{muon}), while in the second member R^* is the rate of background particles counted in the pad during the BC trains.

3.1 Muon Monte Carlo simulation

To evaluate $\delta_{eff}^{(muon)}$ in the standard data taking conditions, a dedicated MC was set which simulates a muon hit occurred in a triggered BC superimposed to a particle background having a rate R_{part} . The fraction of lost muons was evaluated and $\delta_{eff}^{(muon)}$ was calculated from Eq. 3.1. In the triggered BC the time of the muon hit was extracted according to the distribution [2] shown in Fig. 1 (dashed line), while in all the BCs the background hits were extracted as described in Sec. 2.3.

3.2 Muon Monte Carlo results

The Muon MC was run for the BC rate of the LHCb Run1 (20 MHz) and for the future BC rate of 40 MHz. In Fig. 6a the (in)dependence of $\delta_{eff}^{(muon)}$ on μ is shown for two values of δ_c and R_0 . In Fig. 6b the dependence of $\delta_{eff}^{(muon)}$ on δ_c is reported⁶ for the two values of R_0 . It allows to determine the values of $\delta_{eff}^{(muon)}$ corresponding to the measured δ_c values of Table 1. These values are reported in Table 2. The first error on $\delta_{eff}^{(muon)}$ is due to the dispersion of δ_c measured at the five different pairs of luminosity. The second error on $\delta_{eff}^{(muon)}$ was estimated by taking into account the uncertainties on the time distributions of the background and of the muons pulses (bands shown in Fig. 1). The large variations of the errors at $R_0 = 20$ MHz, are due to the undulation induced on $\delta_{eff}^{(muon)}$ by the bunched beam structure (Fig. 6b).

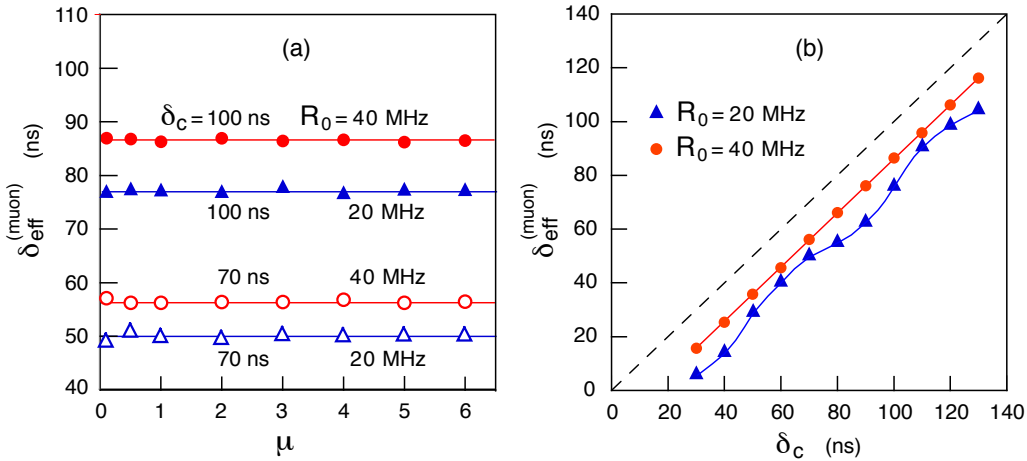


Figure 6. (a) Effective dead-time for muon hit detection for two values of δ_c and R_0 , as a function of the luminosity represented by μ . (b) $\delta_{eff}^{(muon)}$ as a function of δ_c for the two values of R_0 .

⁶A discussion about the different behaviours shown in Fig. 2 and in Fig. 6 is reported in Appendix A.

Table 2. For each region and readout the pad area A (cm²) is shown in the second column. In the third column the average values of δ_c (ns) of Table 1 are reported. The values of $\delta_{eff}^{(muon)}$ (ns), calculated with the muon MC, are reported in the last two columns for a BC rate of 20 MHz and 40 MHz. The first error on $\delta_{eff}^{(muon)}$ is due to the dispersion of δ_c measured at the five different pairs of luminosity while the second error was estimated by taking into account the uncertainties on the time distributions of the background and muon hits (see text).

Region & readout	A	δ_c	$\delta_{eff}^{(muon)}$	
			$R_0 = 20$ MHz	$R_0 = 40$ MHz
M1 R2 cathode	5	$102 \pm 4 \pm 1$	$79 \pm 5 \pm 5$	$89 \pm 4 \pm 2$
M1 R3 cathode	20	$91 \pm 2 \pm 2$	$65 \pm 3 \pm 4$	$77 \pm 2 \pm 2$
M1 R4 anode	80	$71 \pm 4 \pm 1$	$51 \pm 3 \pm 2$	$58 \pm 3 \pm 2$
M2 R1 cathode	11.7	$87 \pm 4 \pm 2$	$61 \pm 4 \pm 3$	$73 \pm 3 \pm 2$
M2 R1 anode	15.6	$73 \pm 7 \pm 1$	$52 \pm 5 \pm 1$	$60 \pm 6 \pm 2$
M2 R2 cathode	23.5	$82 \pm 3 \pm 2$	$57 \pm 3 \pm 2$	$68 \pm 3 \pm 2$
M2 R2 anode	31.25	$68 \pm 3 \pm 2$	$49 \pm 2 \pm 2$	$54 \pm 2 \pm 2$

The muon detection efficiency of a pad is equal to $1 - \delta_{eff}^{(muon)} R^*$ where R^* is the background rate of the pad measured during the duty cycle (70 %) of LHC.

3.3 Muon hit inefficiency in the past and future running conditions

The results reported in Table 2 allow to assess the FE performance in the past runs and predict its behaviour at the high rates foreseen in the future high-luminosity upgrade conditions. For this purpose we express the muon detection efficiency (Eq. 3.1) of a pad as a function of the rate of background particles (R_{part}) hitting the pad:

$$\epsilon_{muon} = \frac{R_{muon}^*}{R_{muon}} = 1 - \delta_{eff}^{(muon)} R^* = 1 - \delta_{eff}^{(muon)} \frac{R_{part}}{1 + \delta_{eff} R_{part}} \quad (3.2)$$

where R_{part} is the particle rate on the pad during the duty cycle (70 %) of LHC and δ_{eff} is a function of δ_c (Fig. 2b). Taking into account the values of δ_c and $\delta_{eff}^{(muon)}$ reported in Table 2, Eq. 3.2 allows to calculate the muon detection efficiency as a function of R_{part} , for the seven considered regions and readout. This efficiency is usually reported as a function of the particle rate per cm² $\mathcal{R}_{part} = 0.7 R_{part} / A$, where $0.7 R_{part}$ is the particle rate on the pad averaged on the running time and A is the pad area reported in Table 2.

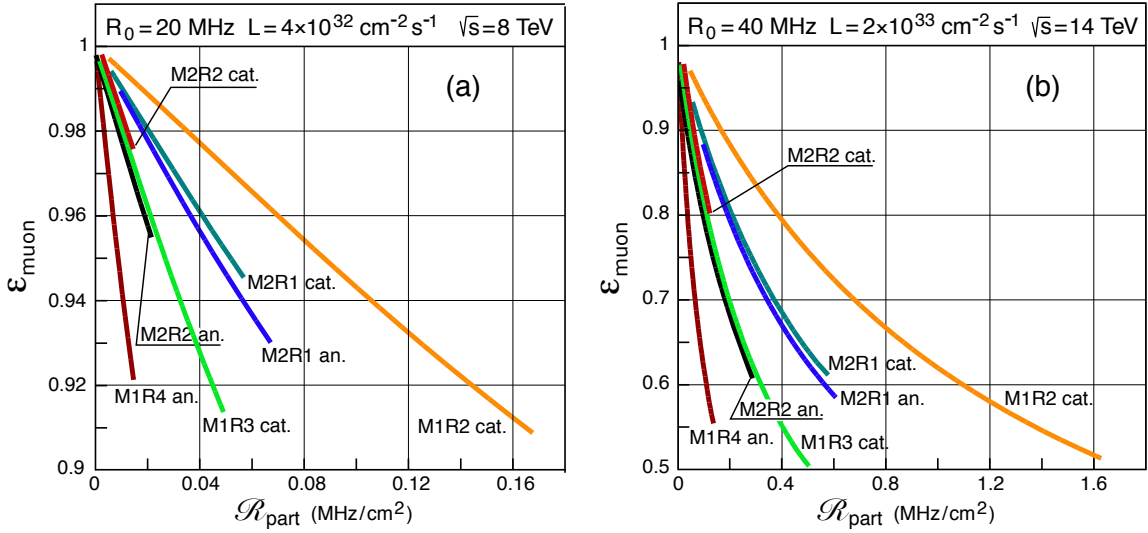


Figure 7. Muon detection efficiency of a single FE for the seven considered regions and readout (monogaps in M1 and bigaps in M2), as a function of the rate per unit area. The past experimental conditions are shown in (a). The future conditions reported in (b) were extrapolated from the experimental data taken at $R_0 = 20$ MHz and $\sqrt{s} = 8$ TeV. An overall factor 1.64 was applied to the expected rates to take into account the increase of \sqrt{s} from 8 TeV to 14 TeV. The curve segments correspond to the interval of \mathcal{R}_{part} observed (a) and expected (b) in the different regions.

In Fig. 7 the muon detection efficiency for the seven considered regions and readout is reported as a function of \mathcal{R}_{part} . In Fig. 7a the curve segments correspond to the effective R^* intervals measured at the LHC pp centre-of-mass energy, $\sqrt{s} = 8$ TeV with $R_0 = 20$ MHz and luminosity $L = 4 \times 10^{32} \text{ cm}^{-2} \text{ s}^{-1}$. In Fig. 7b the curve segments are calculated for $R_0 = 40$ MHz and $L = 2 \times 10^{33} \text{ cm}^{-2} \text{ s}^{-1}$ and an overall factor 1.64 was applied to the expected rates to take into account the increase of \sqrt{s} from 8 TeV to 14 TeV.

Referring to the conditions of Fig. 7b, the number of pads irradiated with \mathcal{R}_{part} MHz/cm² is reported in Fig. 8. The results presented in Fig. 7b and in Fig. 8 show that in the future running conditions the inefficiency due to dead-time would be a limiting factor to the operation of MWPCs belonging to all the regions of station M1 and to the inner region of station M2. Unacceptably poor FE efficiencies are expected in a relatively small zone of these regions, near the beam pipe, where the rate of background (and of good muons) is higher. This effect contributed to the decision [8] of removing station M1 in the upgraded detector for future high-luminosity runs at 14 TeV. Regarding the inner part of M2, the effect of adding an additional shielding around the beam pipe has been studied [8] and other interventions on the detector configuration are under investigation.

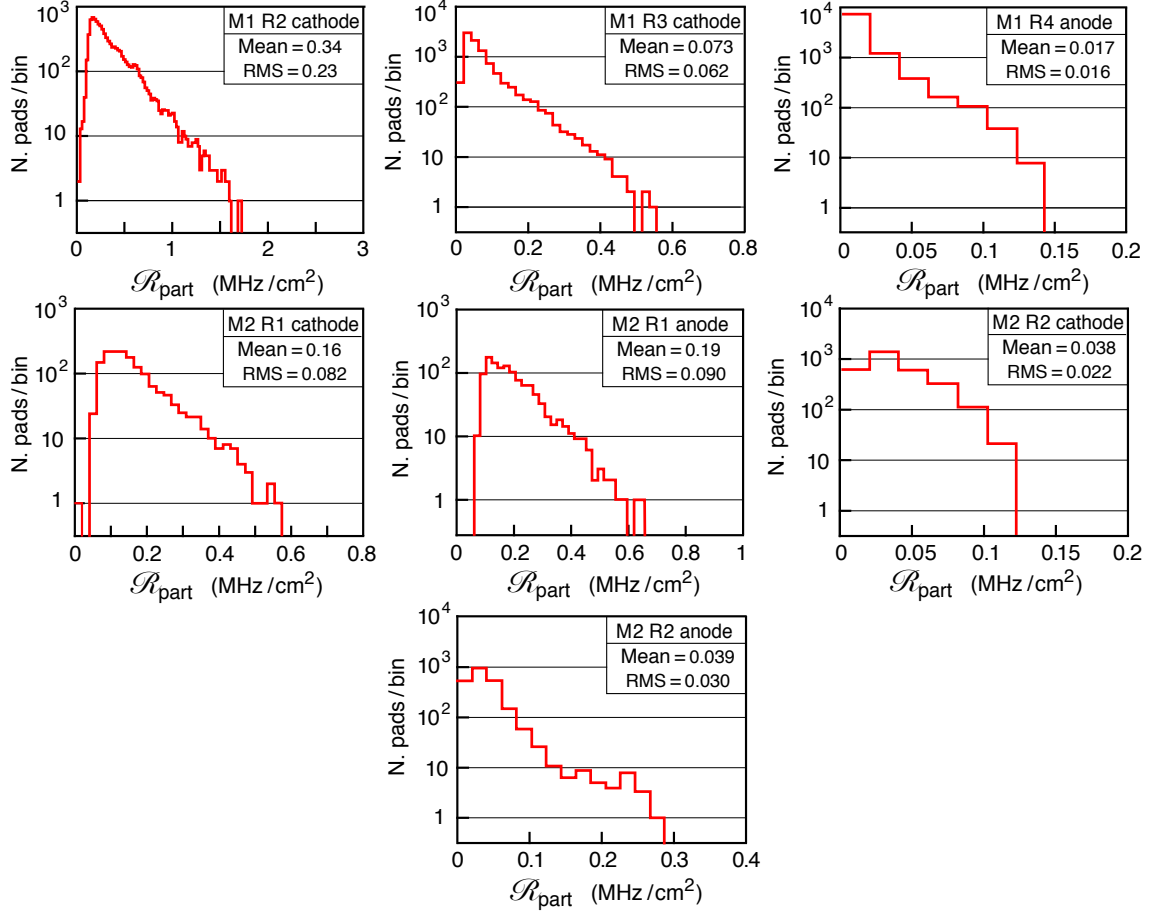


Figure 8. Expected number of pads per bin of \mathcal{R}_{part} in the seven considered regions and readouts, at a luminosity of $2 \times 10^{33} \text{ cm}^{-2}\text{s}^{-1}$ and at $\sqrt{s} = 14 \text{ TeV}$. The distributions were extrapolated from the experimental data taken at $R_0 = 20 \text{ MHz}$ and $\sqrt{s} = 8 \text{ TeV}$. An overall factor 1.64 was applied to the expected rates to take into account the increase of \sqrt{s} from 8 TeV to 14 TeV.

4. Conclusions

The dead-time δ_c of the front-end electronics of stations M1 and M2 of the LHCb muon detector was determined from the experimental background rates measured at different luminosities by free-running front-end scalers. The values obtained range between $\sim 70 \text{ ns}$ and $\sim 100 \text{ ns}$, with the dead-time of the cathode pad readout being systematically larger than that of the anode pads. These results allow to determine the muon detection inefficiency of a front-end channel due to the dead-time, which is the largest contribution to the detector inefficiency in station M1 and in the inner regions of M2. The muon detection inefficiency was evaluated as a function of the background rate per unit area of the pad for the LHCb Run1 bunch-crossing rate of 20 MHz and for the future condition when LHCb will run at a bunch-crossing rate of 40 MHz, at $\sqrt{s} = 14 \text{ TeV}$ and at a luminosity of $2 \times 10^{33} \text{ cm}^{-2}\text{s}^{-1}$. The large front-end inefficiencies expected in the future conditions contributed to the decision of eliminating the station M1 and inserting an additional shielding around the beam pipe upstream of the inner region of station M2.

A. Dead-time effect on background counting and muon detection

In the free-running front-end counters the hit of a particle generated in the current BC can be lost because of the dead-time generated by a particle belonging to a preceding BC or by a particle belonging to the current BC. When the luminosity is decreased, the time interval between two BCs with interacting protons increases so that the counting losses due to preceding BCs become negligible when $L \rightarrow 0$. This is not true for the counting losses due to particles belonging to the current BC. In fact when $L \rightarrow 0$ the number of interactions in the considered BC is $n_{int} = 1$ and the average number of particles hitting the pad is $\omega \neq 0$. Therefore when $L \rightarrow 0$ the fraction of lost particles $R_{lost}/R_{part} = (R_{part} - R^*)/R_{part}$ tends to a non-zero limit⁷:

$$\lim_{L \rightarrow 0} \frac{R_{lost}}{R_{part}} = \lim_{L \rightarrow 0} \frac{R_{part} - R^*}{R_{part}} = \lim_{L \rightarrow 0} (\delta_{eff} R^*) \neq 0 \quad (\text{A.1})$$

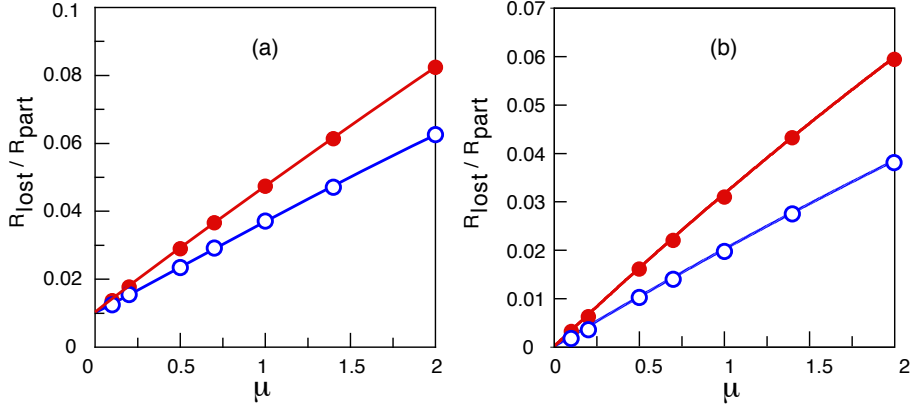


Figure 9. MC results on the ratio between the rate of lost particle and the rate of hitting particles as a function of μ for $\omega = 0.02$; (a) refers to background particles counted with the free-running scalers (see text) while (b) refers to muons counted in a 25 ns triggered gate (standard data taking situation). Open (full) points correspond to $\delta_c = 70$ (100) ns.

As shown in Fig. 9a this effect is correctly predicted by the MC. On the other hand when $L \rightarrow 0$ also $R^* \rightarrow 0$ so that the last equality in Eq. A.1 implies that $\delta_{eff} \rightarrow \infty$. This explains the behaviour of δ_{eff} shown in Fig. 2a.

In the standard data taking the situation is quite different: the muon hit is acquired during a triggered gate of 25 ns. If in this gate the muon hit is cancelled by the dead-time of a background hit generated and detected in the same BC, a hit is counted. As a consequence, the fraction of muon hits lost depends only on the events belonging to the preceding BC and goes to 0 when $L \rightarrow 0$. Therefore $\delta_{eff}^{(muon)}$ results, as expected, to be independent of μ . As shown in Fig. 9b this effect is correctly predicted by the MC.

⁷If $\omega \ll 1$, which is the present case, this limit is equal to $\omega/2$.

References

- [1] A. Augusto Alves Jr. et al., *The LHCb Detector at the LHC*, *JINST* **3** S08005 (2008).
- [2] A. Augusto Alves Jr. et al., *Performance of the LHCb muon system*, *JINST* **8**P02022 (2013).
- [3] G. Graziani et al. *Study of the LHCb Muon Detector performance using 2010 beam data*, CERN-LHCb-PUB-2011-027, <http://cds.cern.ch/record/1408794>, CERN, Geneva Switzerland
- [4] G. Bencivenni et al., *Advances in triple-GEM detector operation for high-rate particle triggering*, *Nucl. Instrum. Meth. A* **513** (2003) 264.
- [5] LHCb collaboration, *LHCb muon system: Second Addendum to the Muon System Technical Design Report*, CERN-LHCC-2005-012, CERN, Geneva Switzerland (2005).
- [6] W. Bonivento et al., *Development of the CARIOCA front-end chip for the LHCb muon detector*, *Nucl. Instrum. Meth. A* **491** (2002) 233.
- [7] D. Pinci, *Performance of the Muon MWPC in high luminosity runs*, LHCb-PUB-2013-005, CERN, Geneva Switzerland (2013).
- [8] LHCb Collaboration, *LHCb PID Upgrade Technical Design Report*, CERN-LHCC-2013-022. CERN, Geneva Switzerland (2013).